GEOPHYSICS, VOL. 67, NO. 1 (JANUARY-FEBRUARY 2002); P. 156–166, 9 FIGS., 3 TABLES.
10.1190/1.1451454

Arbitrary source and receiver positioning in finite-difference schemes using Kaiser windowed sinc functions

Graham. J. Hicks*

ABSTRACT

In finite-difference methods a seismic source can be implemented using either initial wavefield values or body forces. However, body forces can only be specified at finite-difference nodes, and, if using initial values, a source cannot be located close to a reflecting boundary or interface in the model. Hence, difficulties can exist with these schemes when the region surrounding a source is heterogeneous or when a source either is positioned between nodes or is arbitrarily close to a free surface.

A completely general solution to these problems can be obtained by using Kaiser windowed sinc functions to define a small region around the true source location that contains several nodal body forces. Both monopole and dipole point sources can be defined, enabling many source types to be implemented in either acoustic or elastic media. Such a function can also be used to arbitrarily locate receivers. If the number of finite-difference nodes per wavelength is four or more (and with a source region half-width of only four nodes) this scheme results in insignificant phase errors and in amplitude errors of no more than 0.1%. Numerical examples for sources located less than one node from either a free surface or an image source demonstrate that the scheme can be used successfully for any surface–source or multisource configuration.

INTRODUCTION

Finite-difference methods for simulating seismic wavefields are widely used for both modeling and migration/inversion purposes. Since the memory requirements and computational costs of such simulations are significant, it is desirable that as coarse a finite-difference grid as possible is used. Finite-difference schemes that require a minimum of only three or four nodes per wavelength have been developed for the time domain (Dablain, 1986; Holberg, 1987; Cole, 1994) and for the frequency domain (Pratt and Worthington, 1990; Jo et al., 1996; Štekl and Pratt, 1998). However, a common problem with implementing such schemes is that the source and receiver locations may not correspond with those of the modeling nodes and/or they may not be located in homogeneous or smoothly varying parts of the model.

Two main techniques exist for representing seismic sources in finite-difference schemes: as initial values on a boundary or as body forces. These yield the initial value method and the forcing function method, respectively (Sun and McMechan, 1987). The two methods place different restrictions on where a source may be located in the finite-difference model.

In the initial value method an analytic solution to the wavefield in the region of the source is inserted into the finite-difference grid (Alterman and Karal, 1968). This restricts the method to situations for which analytic solutions exist (i.e., normally this imposes a condition of homogeneity in the source region). For these situations this method guarantees that the wavefield close to the source is modeled accurately. Furthermore, because the sources themselves are not represented on the finite-difference grid, they can be arbitrarily positioned with respect to the grid. To prevent artifacts arising from backscattered events diffracted by the source region, the source must be defined at two time steps. During the first step the source wavefield is inserted at the finite-difference nodes surrounding the source location; during the second step the finite-difference scheme is turned on in this region so that it does not reflect backscattered arrivals.

Separating the initial source function from later events that pass through the source region is a problem if (1) the model is not smoothly varying close to the source [i.e., a distance from the surface where the source wavefield is inserted that is greater than the spatial extent of the finite-difference stencil (Robertsson et al., 1996) and is at least as large as half a complete wavelet, so that the initial values are not affected by backscattered arrivals] or if (2) the source is similarly close to a free surface. Although the appropriate analytic solution for a source near a free surface (or other interface) can be used,

Manuscript received by the Editor August 2, 2000; revised manuscript received March 6, 2001.
*Formerly Queen's University, Department of Geological Sciences, Kingston, Ontario K7L 3N6, Canada; presently TotalFinaElf Exploration UK, Geoscience Research Centre, 33 Cavendish Square, London W1G 0PW, U.K. E-mail: graham.hicks@tfeeuk.co.uk.

converted waves, surface waves, and all surface multiples other than the source ghost are then not modeled. Difficulties can therefore be expected when modeling with many common acquisition geometries, including downhole simulations, ocean-bottom seismometer recordings, and very-near-surface reflection and refraction simulations. No attempts to adapt the initial value method for use in frequency-domain schemes exist. Indeed, such a task may be impossible because the conventional initial value method requires separate time steps.

The forcing function method is easily implemented in both time-domain and frequency-domain schemes. In the forcing function method, body forces are explicitly included in the equation of motion (Alterman and Aboudi, 1970; Aboudi, 1971). The source terms then drive the propagation of the wavefields. The main disadvantages of this method are that the source terms add complexity to the resulting finite-difference equations, causing reduced numerical stability (Alford et al., 1974), and, because of the singular nature of the wavefield at the source location, large numerical errors are common close to the source. A further, potential disadvantage is that body forces may only be specified at finite-difference node locations. Sources have therefore traditionally been restricted to being located at finite-difference nodes.

To represent arbitrarily positioned sources using the forcing function method, one must find the combination of nodal source terms that are equivalent to a source located at the desired internodal location. The simplest solution is to increase the spatial extent of the source so that it contributes to all nodes less than one node spacing from its center (Aboudi, 1971). The source can then be arbitrarily positioned, but it is no longer a true point source.

Two methods for determining a combination of nodal source terms that are equivalent to an arbitrarily located point source have been presented. Landrø et al. (1993) describe how the desired source terms can be estimated by an inversion that seeks to minimize the differences, at a horizontal surface below the source, between the finite-difference solution and an analytic solution. The main limitations of this technique are (1) an appropriate analytic solution must exist and (2) the inversion procedure must be performed separately for each source. Mittet and Arntsen (1999) describe a scheme in which the source contributions at the nodes are determined by designing an optimal phase-shift operator. According to the authors, a unique operator needs to be determined for each possible internodal source location (although these can be computed once and then stored). The scheme I describe is a refinement of the method of Mittet and Arntsen (1999), allowing a single operator to be used for all arbitrary source locations and significantly simplifying the optimization of this operator. I also extend the method so that it can be used near a free surface and describe how it can be combined with the work of Aboudi (1971) to implement a variety of source mechanisms in an elastic medium.

Both the initial value method and the inversion method of Landrø et al. (1993) are solutions only for arbitrary positioning of sources; a different solution to the problem of arbitrary positioning of receivers must be found. Although simple interpolation can be applied successfully between time-domain traces simulated at neighboring nodes, in the frequency domain this approach requires that the data be converted to amplitudes and phases, which vary smoothly in space (whereas the real and imaginary components of a complex wavefield are sinusoidal in space). However, there are problems in uniquely transforming the interpolated amplitudes and phases back to complex wavefield values, especially in the presence of potential cycle skipping. Moreover, in many migration/inversion applications, data residuals, recorded at the receivers, are back-propagated through the model. Hence, for this modeling step the receivers become the sources. To maintain source–receiver reciprocity, the representation of sources and receivers, both arbitrarily located, should be treated in an identical manner.

I present a method for arbitrary positioning of both sources and receivers using spatially distributed point body forces or point receivers. By simultaneously using more than one source or receiver, source and receiver arrays can be simulated. Similarly, by simultaneously modeling a source and a corresponding image source (i.e., a dipole), a ghost-generating free surface can be simulated (Cunha, 1993). Numerical results are presented for the latter application, which can be seen as a specific case of the former. Results generated in this manner are compared with those obtained when a free surface is explicitly included in the finite-difference scheme. Results are also presented for a source located between the free surface and the next row of nodes.

THEORY

For simplicity I begin by considering acoustic modeling in 1-D space. The equation of motion for inhomogeneous media, on which the forcing function method of finite-difference propagation is based, can be given as

$$\left[\frac{1}{K(x)}\frac{\partial^2}{\partial t^2} - \frac{\partial}{\partial x}\left(\frac{1}{\rho(x)}\frac{\partial}{\partial x}\right)\right]p(x,t) = f(x,t) \qquad (1)$$

in the time domain or as

$$\left[\frac{\omega^2}{K(x)} + \frac{\partial}{\partial x}\left(\frac{1}{\rho(x)}\frac{\partial}{\partial x}\right)\right]P(x,\omega) = -F(x,\omega) \qquad (2)$$

in the frequency domain. The model is characterized by spatial variations of density $\rho(x)$ and the bulk modulus $K(x)$; the source function $[f(x,t)$ or $F(x,\omega)]$ and the resulting pressure field $[p(x,t)$ or $P(x,\omega)]$ are described in either the time–space or frequency–space domain. I define x with units of finite-difference node spacings, so that all formulas are independent of the physical grid spacing.

I now consider the source function in either equation (1) or (2) and hence in either the time–space or frequency–space domain. For a point source, the source function is defined as $f(x) = S\delta(x)$, where $\delta(x)$ is a spatial delta function, and S, defined in either the time or frequency domain, determines the temporal variation of the source. The resulting source function is then sampled on a finite-difference grid, yielding a discrete version of $f(x)$:

$$f_n = S\delta(n+\alpha), \qquad (3)$$

where $-0.5 < \alpha \le 0.5$ and n is an integer, such that $x = n + \alpha$ is the distance from the source in finite-difference nodes.

For the source function to be adequately sampled by the finite-difference grid, it is necessary to replace $\delta(x)$ with a band-limited version of itself, $\tilde{\delta}(x)$, that has a wavenumber spectrum as close as possible to that of $\delta(x)$ for all wavenumbers less than the Nyquist wavenumber, i.e., for all $k < \pi$, and as close as possible to zero for all $k > \pi$. The ideal band-limited delta

function is therefore a sinc function with a period of one-half, defined as

$$\mathrm{sinc}(x) \equiv \frac{\sin(\pi x)}{\pi x} \tag{4}$$

and is depicted by the black line in Figure 1. If the source is coincident with a finite-difference node (i.e., $\alpha = 0$), then the discrete source function f_n will be nonzero only for $n = 0$ [since $\mathrm{sinc}(x) = 0$ for x equal to all nonzero integers]. But if the source is located between nodes, the discrete source function will be nonzero for all n (i.e., a source function of infinite nonzero spatial extent is defined). It is therefore necessary to apply a spatial window to $\mathrm{sinc}(x)$, forming a discrete, band-limited, spatially finite approximation of a delta function d_n. The discrete source function is then given by

$$f_n = S\,d_n = S[W(n+\alpha)\,\mathrm{sinc}(n+\alpha)], \tag{5}$$

where W represents a windowing function. We wish to design W so that, for a source function with the smallest possible spatial extent, the wavenumber domain properties of d_n are, within the wavenumber range of interest, as close as possible to those of the band-limited $\tilde{\delta}(x)$.

The windowing operator is determined by the type of function used and its width. Provided the windowing function is symmetric about $x = 0$, the k-domain phase response of d_n will be near zero for all $k < \pi$ (and exactly zero if $\alpha = 0.0$ or 0.5), but its amplitude response may vary significantly from the desired value of unity. The simplest form of windowing is to truncate $\mathrm{sinc}(x)$ at $x = \pm r$ (i.e., apply a rectangular window of half-width r). However, even if r is large, this type of windowing significantly corrupts the amplitude spectra of d_n, associated with Gibbs' phenomenon.

Kaiser (1974) proposes a family of simple, yet near-optimal, windowing functions for the design of finite impulse response (FIR) filters. These windows are given by

$$W(x) = \begin{cases} \dfrac{I_0\left(b\sqrt{1-(x/r)^2}\right)}{I_0(b)} & \text{for } -r \le x \le r \\ 0 & \text{otherwise} \end{cases}, \tag{6}$$

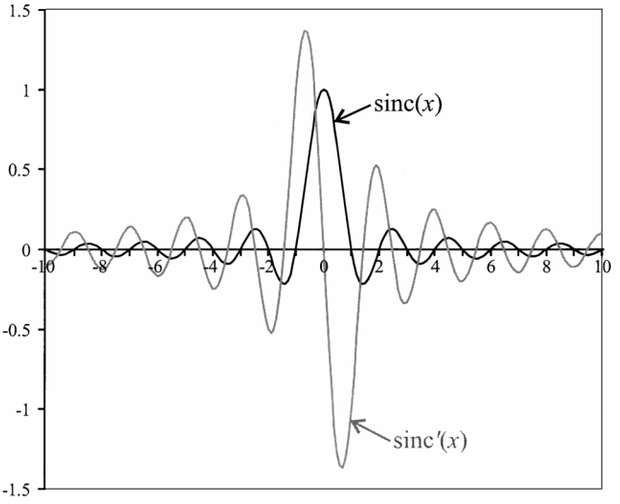

FIG. 1. The sinc function as defined by equation (4) and its first spatial derivative, given by equation (9).

where r is the window half-width and I_0 is the zero-order modified Bessel function of the first kind. Other common windowing functions have a fixed shape and are therefore optimal only in specific situations, but the shape of a Kaiser window can be altered by changing a single parameter, b. For $b = 0$ the Kaiser window reduces to a rectangular window; as $b \to \infty$, a delta function is obtained. Two useful Kaiser windows ($b = 4.14$ and $b = 6.31$), both with half-widths of $r = 4$ node spacings, and the resulting windowed sinc functions are shown in Figure 2.

The optimal windowing function preserves the wavenumber response of $\mathrm{sinc}(x)$, as given in equation (4), and hence has an amplitude spectrum of unity and a phase spectrum of zero across the wavenumber range of interest, i.e., the one for which $D(k) = 1$, where $D(k)$ is the complex wavenumber response of d_n, which is given by

$$D(k) = \sum_{n=-r}^{r} d_n\, e^{ik(n+\alpha)}. \tag{7}$$

The variation of $|D(k)|$ with wavenumber for Hanning (raised half-cosine), Hamming (stretched, raised half-cosine), Blackman (raised half-cosine with second harmonic), and two different Kaiser windows is shown in Figure 3 (for a window half-width of $r = 4$ and internode displacement of $\alpha = 0.5$). As k increases, the error in the spectral amplitude of d_n tends to increase because of the difficulty of maintaining the correct wavenumber properties when a spatially limited window is used. All the types of window used result in extremely large spectral amplitude errors at large wavenumbers ($\frac{3}{4}\pi < k < \pi$), but reasonably small errors can be obtained for $k \le \frac{2}{3}\pi$. This upper wavenumber limit corresponds to three or more samples per wavelength, which is the minimum nodal sampling required for accurate modeling using high-order finite-difference schemes. The Hanning window results in the largest deviations from the desired spectral amplitude of unity; the Hamming window yields spectral errors that are reasonably small for all $k < 0.58\pi$; and the Blackman window yields errors that are very small at small wavenumbers but that quickly become extremely large once $k > 0.42\pi$.

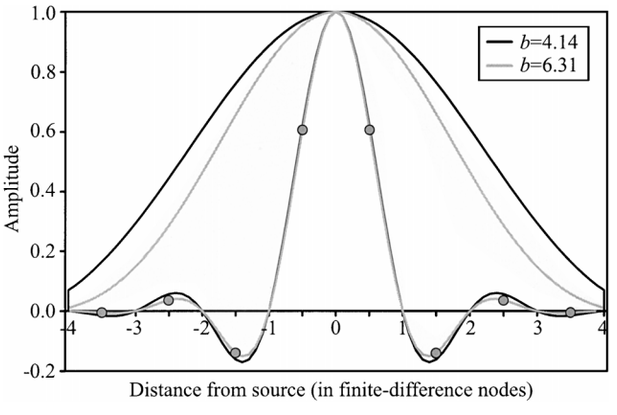

FIG. 2. Kaiser windowing functions and the corresponding windowed sinc functions for two windows with a half-width of $r = 4$ and with windowing parameters $b = 4.14$ (black line) or $b = 6.31$ (gray line). Circles indicate the eight nonzero values of d_n obtained when $r = 4$, $b = 6.31$, and $\alpha = 0.5$.

By varying the parameter b, the Kaiser window can be tuned so that, over a specified range of wavenumbers, the minimum possible spectral errors are achieved. This tuning can be performed via an optimization of the spectral properties of d_n. Since we are interested in obtaining errors that are as small as possible for all internodal source positions α and all wavenumbers of interest, I seek to minimize the minimax (or Chebyshev) error function,

$$\varepsilon = \max_{\substack{\alpha\in -0.5<\alpha\le 0.5 \\ k\in 0\le k\le k_{max}}} |D(k)-1|. \tag{8}$$

The wavenumbers of interest are given by $k=\omega/v$, where v is the velocity at the source and ω is a modeled angular data frequency. This is a similar approach to that which can be used to optimally design low-pass filters (e.g., Oppenheim and Schafer, 1989; pp. 462–469), except that we are only interested in optimizing the properties of the passband.

The two values of b used in Figure 3 were obtained by minimizing ε with either $k_{max}=\frac{2}{3}\pi$ or $k_{max}=\frac{1}{2}\pi$. Consequently, the first Kaiser window ($b=4.14$) yields errors that are <0.008 for all $k\le\frac{2}{3}\pi$; the second Kaiser window ($b=6.31$) yields errors that are <0.0012 for all $k\le\frac{1}{2}\pi$. In the following section I show that both these levels of error are acceptable when equation (5) is used to position sources between finite-difference nodes. However, if finite-difference modeling is implemented in the frequency–space domain, even greater accuracy could be achieved by using a different optimum windowing parameter for each wavenumber corresponding with each single-frequency source component.

In Figure 4 the effect of $|D(k)|$ of varying α, which represents the internodal positioning of the source, is depicted for a fixed windowing parameter of $b=4.14$. The largest errors are for $\alpha=0.5$, a finding that I also confirmed by numerical tests using different internodal source locations. Therefore, if modeling errors are acceptable for $\alpha=0.5$, they will be acceptable for any α. Hence, we can use the same windowing function for all sources (and receivers) regardless of their internodal location. Furthermore, it is not necessary to actually perform the search over α when evaluating equation (8). Instead, a fixed value of $\alpha=0.5$ can be used.

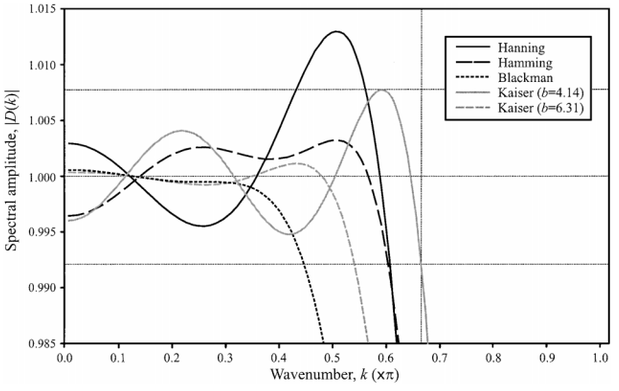

FIG. 3. The wavenumber spectrum of d_n between $k=0$ and the Nyquist wavenumber for five different windowing functions in equation (5). The desired spectral amplitude is one. The window half-width used is $r=4$, and the internodal displacement is $\alpha=0.5$.

So far I have only considered the errors in $D(k)$ for a window of half-width $r=4$. Clearly, errors should be reduced if we increase r, but it is necessary to keep r as small as possible because the windowed sinc function will not be optimal if model parameters are not constant in the region of the model included in the window (the source region). This is because the desired wavefield is constructed from the superposition of wavefields emanating from each of the nodes inside the source region; hence, the velocity across this region must be constant so these individual wavefields interfere correctly, and both velocity and density must be constant to ensure that the amplitudes of the individual wavefields are correctly proportioned. Furthermore, because the wavefield inside this region is not accurately modeled, receivers should not be located less than r finite-difference nodes from the source. In Table 1 for maximum-wavenumbers of interest $k_{max}=\frac{1}{2}\pi$ and $k_{max}=\frac{2}{3}\pi$, I give the optimum Kaiser windowing parameters b and the corresponding wavenumber domain errors ε for ten different window half-widths. The trade-off between window size and error can be easily appreciated. Also note that numerical results presented later in this paper demonstrate that errors of less than about $\varepsilon=10^{-3}$ are negligible.

Multipole sources

Nonradially symmetric sources can be modeled by replacing $\delta(x)$ in equation (3) with a higher order spatial derivative of itself. For example, the forcing function for a dipole source is given by using $\delta'(x)$. As before, for the discrete source function to be adequately sampled, this function must be replaced by an equivalent one of finite bandwidth, where this function is simply the corresponding spatial derivative of the sinc function defined in equation (4). For example, the first spatial derivative of $\mathrm{sinc}(x)$, as depicted in Figure 1, is given by

$$\mathrm{sinc}'(x) \equiv \frac{\cos(\pi x)-\mathrm{sinc}(x)}{x}. \tag{9}$$

As before, windowing must also be applied to obtain a source function of finite spatial extent:

$$f_n = S\,d'_n = S\,[W(n+\alpha)\,\mathrm{sinc}'(n+\alpha)]. \tag{10}$$

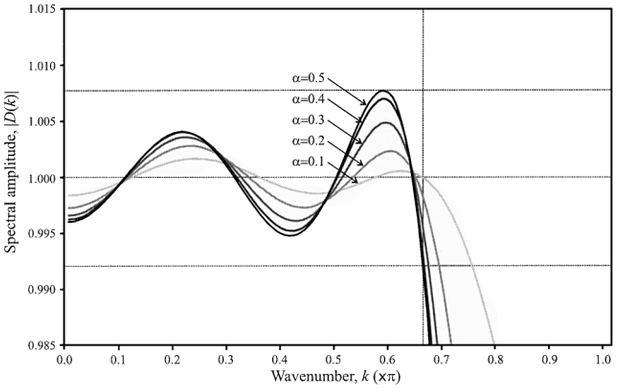

FIG. 4. The wavenumber spectrum of d_n between $k=0$ and the Nyquist wavenumber for a Kaiser window with $b=4.14$ and for five different values of α, corresponding to different internodal source locations. The largest deviations from the desired spectral amplitude of unity are for $\alpha=0.5$, i.e., for a source located midway between finite-difference nodes.

Optimum Kaiser windowing functions can be obtained by minimizing the difference between the wavenumber domain properties of $\text{sinc}'(x)$ and $\delta'(x)$. This is achieved in a manner identical to that described for a monopole source, except that since the wavenumber domain response of $\delta'(x)$ is ik, the term $|D(k)-1|$ in equation (8) must be replaced with $|D'(k)-ik|$, where $D'(k)$ is the Fourier response of d'_n. The resulting optimum windowing parameters and their corresponding maximum wavenumber domain errors are given in Table 2. Note that the errors for a dipole source are slightly larger than those obtained for a monopole source (Table 1). This can be understood by examining Figure 1 in which the envelope of $\text{sinc}'(x)$ is seen to be wider than $\text{sinc}(x)$, so a larger window is required to achieve a similar level of accuracy. Also of interest in Figure 1 is that for integer values of x (i.e., when $\alpha=0$), $\text{sinc}'(x)$ has its largest possible values (except at $x=0$). Hence, for a dipole source the maximum wavenumber errors occur when $\alpha=0$.

Receivers

The value of a discretely sampled wavefield at an arbitrary location can be determined by using the same optimally windowed sinc function as used in equation (5):

$$R=\sum_{n=-r}^{r} p_n\, d_n, \tag{11}$$

where p_n is the finite-difference wavefield solution at finite-difference nodes corresponding with $-r\le n\le r$ and R is the receiver response (in the same domain and with the same units as p_n). Following equation (10) the extension to nonomnidirectional receivers is obvious.

Sources and receivers in multidimensional space

The 1-D source function given by equation (5) [or equation (10)] and the receiver response given by equation (11) are easily adapted to higher spatial dimensions by replacing d_n (or d'_n) with the appropriate higher dimensional approximation to $\tilde{\delta}(x)$ [or $\tilde{\delta}'(x)$]. For example, the 2-D version of equation (5) is

$$f_n^{2D}(x,z)=S\,d_n^{2D}(x,z)=S\,d_n(x)\,d_n(z). \tag{12}$$

Elastic modeling in 2-D media

The spatial distribution of body forces required to describe many general source mechanisms in an elastic medium can be obtained by a linear combination of band-limited approximations to $\delta(x)$ and $\delta'(x)$. By replacing the bell-shaped approximation of $\delta(x)$ used by Aboudi (1971) with a Kaiser windowed sinc function, the formulas he presented can be used to define arbitrarily located point sources of many types in an elastic 2-D medium. In this application separate source functions are defined for the horizontally and vertically oriented body forces $(f_n^{2D}(x,z))_x$ and $(f_n^{2D}(x,z))_z$; hence, the 2-D source function $f_n^{2D}(x,z)$ is replaced by the 2-D source function vector $\mathbf{f}_n^{2D}(x,z)$. For example, an explosive (P-wave only) source is given by

Table 1. Optimum Kaiser windowing parameter b and corresponding wavenumber domain error ε for two different maximum wavenumbers of interest k_{max} and ten different window half-widths r.

	$k_{max}=\frac{1}{2}\pi$		$k_{max}=\frac{2}{3}\pi$	
Half-width r	Optimum b	Spectral error ε	Optimum b	Spectral error ε
1	1.24	1.72E-01	0.00	3.52E-01
2	2.94	2.32E-02	1.84	8.46E-02
3	4.53	4.79E-03	3.04	2.50E-02
4	6.31	1.34E-03	4.14	7.97E-03
5	7.91	2.43E-04	5.26	2.83E-03
6	9.42	4.88E-05	6.40	1.04E-03
7	10.95	9.79E-06	7.51	3.49E-04
8	12.53	2.19E-06	8.56	1.03E-04
9	14.09	8.23E-07	9.56	3.53E-05
10	14.18	7.99E-07	10.64	1.14E-05

Table 2. Optimum Kaiser windowing parameters and corresponding spectral errors for the dipole point source given by equation (10). The errors given are the maximum deviations of $D'(k)$ from ik in the parameter space $0\le k\le k_{max}$ and $0.5<\alpha\le 0.5$.

	$k_{max}=\frac{1}{2}\pi$		$k_{max}=\frac{2}{3}\pi$	
Half-width r	Optimum b	Spectral error ε	Optimum b	Spectral error ε
1	0.00	1.57E-00	0.00	2.07E-00
2	3.33	1.97E-01	1.48	5.07E-01
3	4.96	3.39E-02	3.25	1.46E-01
4	6.42	6.81E-03	4.40	4.36E-02
5	7.77	1.52E-03	5.44	1.35E-02
6	9.52	2.46E-04	6.46	4.40E-03
7	11.11	5.29E-05	7.41	1.55E-03
8	12.52	1.40E-05	8.50	4.95E-04
9	14.25	1.06E-05	9.66	1.63E-04
10	16.09	1.02E-05	10.77	6.00E-05

$$\mathbf{f}_n^{2D}(x,z) = \begin{bmatrix} \left(f_n^{2D}(x,z)\right)_x \\ \left(f_n^{2D}(x,z)\right)_z \end{bmatrix}^T = \begin{bmatrix} S\,d_n'(x)\;d_n(z) \\ S\,d_n(x)\;d_n'(z) \end{bmatrix}^T. \tag{13}$$

Note that the asymmetry of d_n' causes the particle motions on either side of the source to be in opposite directions, as required. Surface forces may also be used by combining the formulas of Aboudi (1971) with those given here. The displacements (or particle velocities) at the receiver locations are obtained by applying the 2-D receiver function, given by equations (11) and (12), separately for the horizontal and vertical displacements.

NUMERICAL EXAMPLES

I used the method described in the previous section to position both sources and receivers between finite-difference nodes in a series of numerical examples. The modeling results thus obtained can be compared with those obtained when both the source and the receivers are located at finite-difference nodes. These examples demonstrate that the method is sufficiently accurate for arbitrarily located sources in three different situations: propagation from a single source, propagation from a source and image source pair (dipole), and propagation from a source located close to a free surface.

Errors are wavenumber dependent, so results are presented for monofrequency simulations. The acoustic frequency–space domain, finite-difference code used was developed by Pratt and Worthington (1990) and Štekl (1997). An analytic solution was not used for comparison with modeled data because errors from the source–receiver representation would be combined with the propagation errors. Instead, data modeled with sources and receivers located at finite-difference nodes were compared with the equivalent data modeled with sources and receivers located between nodes.

Single source modeling

Modeling was performed on a finite-difference grid with a nodal spacing of 10 m and a homogeneous velocity of 2000 ms^{-1}. The amplitude and phase of two monofrequency wavefields were sampled by receivers located 50, 100, 150, 200, 250, and 300 m from the source. The modeled values obtained when the source and all the receivers are located at modeling nodes (Figure 5a) are compared with those obtained when the source and receivers are shifted by less than the internodal spacing (Figures 5c–f). To assess the significance of errors from numerical noise and reflections from imperfectly absorbing boundaries, data were also computed with the source and receivers shifted by a single modeling node (Figure 5b). The resulting change in the amplitude and phase of the modeled wavefield is depicted by the first (black) bars in Figure 6, which show that modeling errors are <1% in amplitude and <0.004 radians in phase. A phase error of 0.004 radians corresponds with a timing error of approximately 0.0289 ms at 22 Hz or 0.0110 ms at 58 Hz. These two frequencies correspond with wavenumbers (in units of one over the grid spacing) of 0.22π and 0.58π with approximately 9.1 and 3.4 nodes per wavelength, respectively. These two wavenumbers were chosen because they correspond with maximum errors in $|D(k)|$ for the Kaiser window obtained using $b = 4.14$ (see Figure 3). If the modeling errors obtained using that window are acceptable at these frequencies, they will be acceptable for all $k \le \frac{2}{3}\pi$.

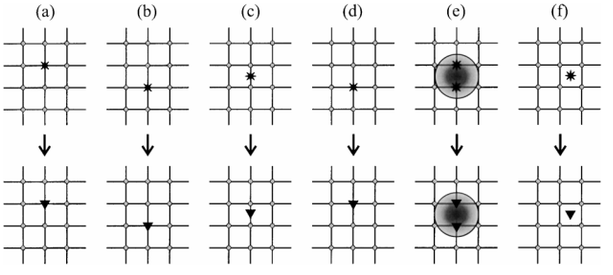

FIG. 5. Different source and receiver positions used to generate the results in Figure 6. Only one of the six receivers is shown. The receivers are located directly below the source. (d) The source–receiver distance is one node spacing less than in all the other panels. (e) The source and receiver have a finite spatial extent, and the active nodes within this region are indicated.

Kaiser windowed sinc functions with half-widths of $r = 4$ were used to locate the source and receivers midway between nodes (Figure 5c). The modeling errors obtained by subtracting these data from those modeled using the configuration in Figure 5a are depicted in Figure 6 (second and third bars) for Kaiser windows of $b = 4.14$ and $b = 6.31$. At 22 Hz, using $b = 6.31$ results in near-zero amplitude and phase errors. Using $b = 4.14$ results in slightly larger errors (although the amplitude errors are still <1% and phase errors are even less significant). At 58 Hz both the amplitude and phase errors are smaller for $b = 4.14$ than they are for $b = 6.31$ (amplitude errors reach 2% and 5%, respectively), and the errors are larger than they were at 22 Hz. These results correspond with the wavenumber domain properties depicted in Figure 3.

These errors may be compared with those obtained if the source is mislocated by 10 m (Figure 5d and the fourth set of bars in Figure 6). Even at 22 Hz, for which 10 m corresponds with only 0.11 of a wavelength, misplacing the source leads to large phase errors; however, amplitude errors are only large close to the source.

Another rough-and-ready way to handle sources and receivers located between nodes is to increase the spatial extent of the sources and receivers so they cover the nodes immediately surrounding their true location. Alterman and Aboudi (1970) and Aboudi (1971) present a bell-shaped approximation of a delta function which can be used in place of $\delta(n+\alpha)$ in equation (3) to implement a source of finite extent. The closest approximation to a point source that can be achieved is that obtained by setting the distance between the center of the source and its surface (the half-width of the source) equal to the finite-difference node spacing. The source will then consist of nonzero body forces at all the nodes less than one node spacing from its center. Hence, for a source located at a finite-difference node, the source function is identical to that obtained using a true delta function. For a source located between nodes in one of the Cartesian directions of the finite-difference grid, body forces are defined at the two nodes closest to the center of the source. If $\alpha = 0.5$ (as in Figure 5e) equal weights of one-half are used at both nodes. The same approach can be used with receivers of finite spatial extent. In contrast to misplacing the source, using sources and receivers of finite spatial extent results in large amplitude errors, especially at high wavenumbers, but phase errors are reasonably small (fifth set of bars

in Figure 6). The amplitude errors result from the slightly deconstructive interference of waveforms from either side of the source and recorded at either side of the receivers.

The last two sets of bars in Figure 6 depict the amplitude and phase errors obtained when the source and receivers are located midway between finite-difference nodes in both the x and z directions (Figure 5f), again using Kaiser windows with $b = 4.14$ or $b = 6.31$. The 2-D windowed sinc function given by equation (12) must now be used. The errors are very similar to those depicted in the second and third bars of Figure 6; surprisingly, the amplitude errors at 22 Hz are even smaller than before. Together these results show that using a single Kaiser windowing function (of half-width $r = 4$), amplitude errors of less than about 2% and phase errors of less than about 0.005 radians can be achieved for all the wavenumbers of interest in finite-difference modeling.

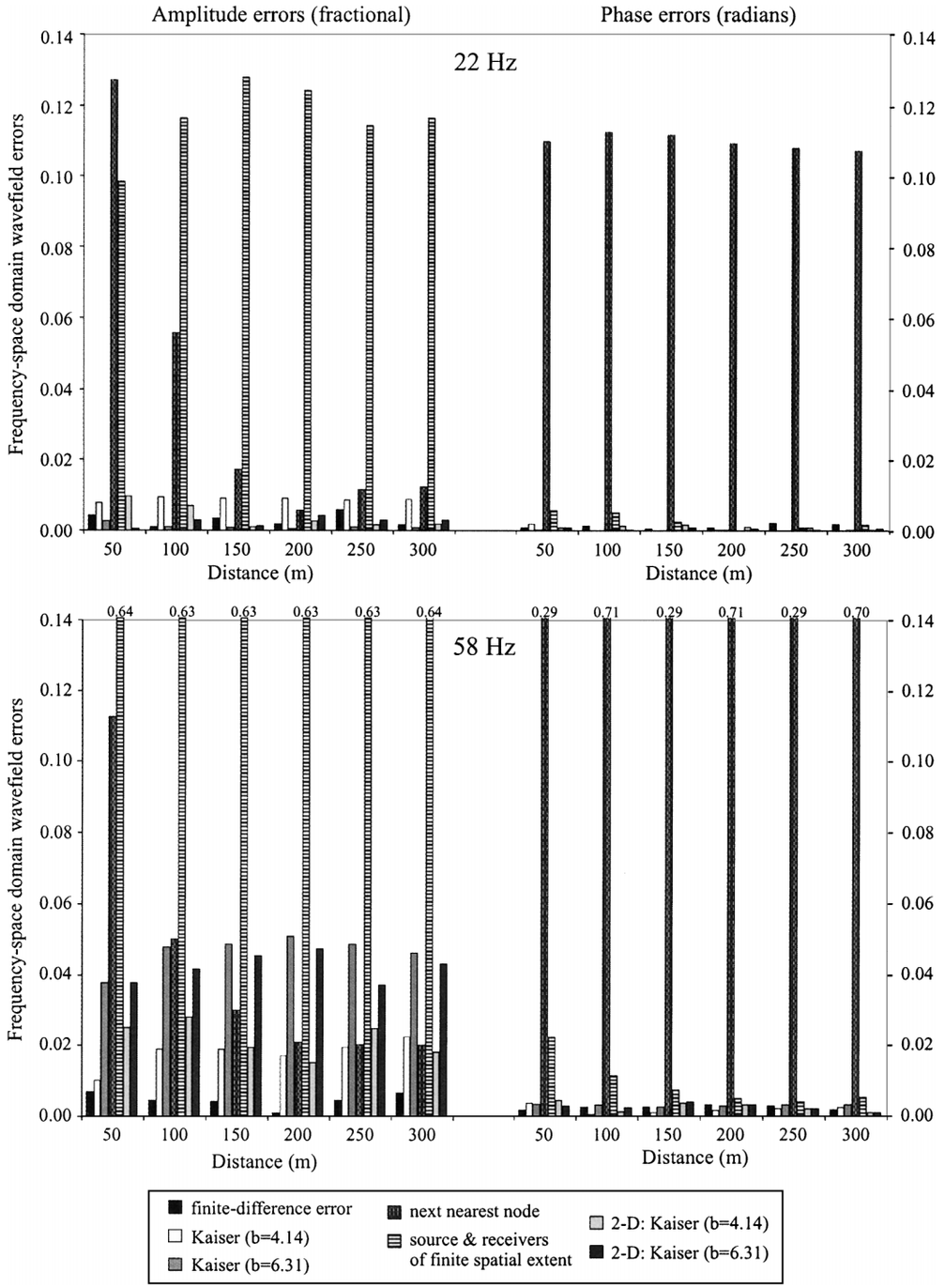

FIG. 6. Amplitude and phase errors at receivers 50–300 m from the source at two frequencies. The errors were calculated from the differences between data obtained using the source and receiver positions depicted in Figures 5b–f with that obtained using the positions depicted in Figure 5a. Where applicable, errors are given for two different Kaiser windows, both with a half-width of $r = 4$.

As discussed in the previous section, it is desirable to use as small a source region as possible. In Figure 7 amplitude and phase errors 250 m from the source are presented for ten different-sized source regions for a source and receiver located midway between modeling nodes. The Kaiser windowing parameters used for the modeling results at 22 Hz and at 58 Hz are the optimal values given in Table 1 for a maximum wavenumber of $\frac{1}{2}\pi$ or $\frac{2}{3}\pi$, respectively. The amplitude errors associated with the source and receiver positioning are less than the modeling errors (first bars) for all $r > 2$ at 22 Hz and for all $r > 5$ at 58 Hz; the corresponding phase errors are less than the modeling errors for all r at 22 Hz and for all $r > 2$ at 58 Hz. Hence, as indicated by Table 1, a smaller source region is required when the maximum wavenumber/frequency of interest is reduced. The choice of r will therefore depend on how large a homogeneous region around the sources/receivers is considered acceptable and on the maximum wavenumber to be modeled. However, I suggest that a source–receiver region half-width of $r = 4$ is probably a good compromise in many situations.

Ghost simulation and modeling with a free surface

I now show that this method can be used in two more problematic situations: (1) when the source is located arbitrarily close to a free surface (as defined in the finite-difference scheme by a zero pressure boundary condition) and (2) when a finely spaced source and image source pair is used to simulate a free-surface ghost. The second of these can be seen as a special case of using multiple sources simultaneously, other possible applications of which are the simulation of source arrays, exploding reflectors, or downhole sources with their attendant tube waves (Kurkjian et al., 1994). However, the use of ghost-generating source pairs requires an especially high level of accuracy because the original source and the image source are of equal and opposite amplitude; thus, any erroneous differences between them will be amplified.

A ghost-generating source pair should be able to simulate the wavelet produced by a single source located close to a free surface. Figure 8 depicts five different ways of simulating a source located half a grid spacing (5 m) below a free surface in a homogeneous (2000 ms^{-1}) half-space. In Figures 8a–c source and image source pairs (dipoles) are depicted. The source ghost-generating surfaces correspond to the lines bisecting the two sources. The thick line in Figures 8d and e represent zero pressure boundaries in the finite-difference scheme. Receivers are located 50, 100, 150, 200, 250, and 300 m below the free surface; consequently they do not coincide with node locations for Figures 8a, d, or e. To position sources and receivers between nodes, a sinc function, windowed using a Kaiser function with

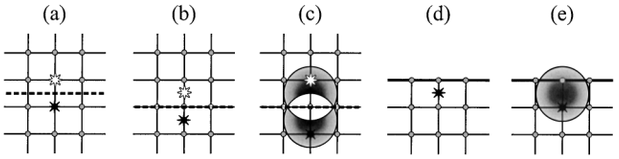

FIG. 8. Different source positions used to generate the results in Table 3. The white stars represent image sources which have an equal and opposite amplitude to the original sources (black stars). The resulting ghost-generating simulated free surfaces are indicated by dashed lines. The thick lines in (d) and (e) represent free-surface boundary conditions in the finite-difference scheme. The distance between the source and the free surface (explicit or simulated) is one-half grid spacing (5 m). In (c) and (e) sources with half-widths of one node spacing are represented, and the active nodes are indicated. The receivers are located directly below the source.

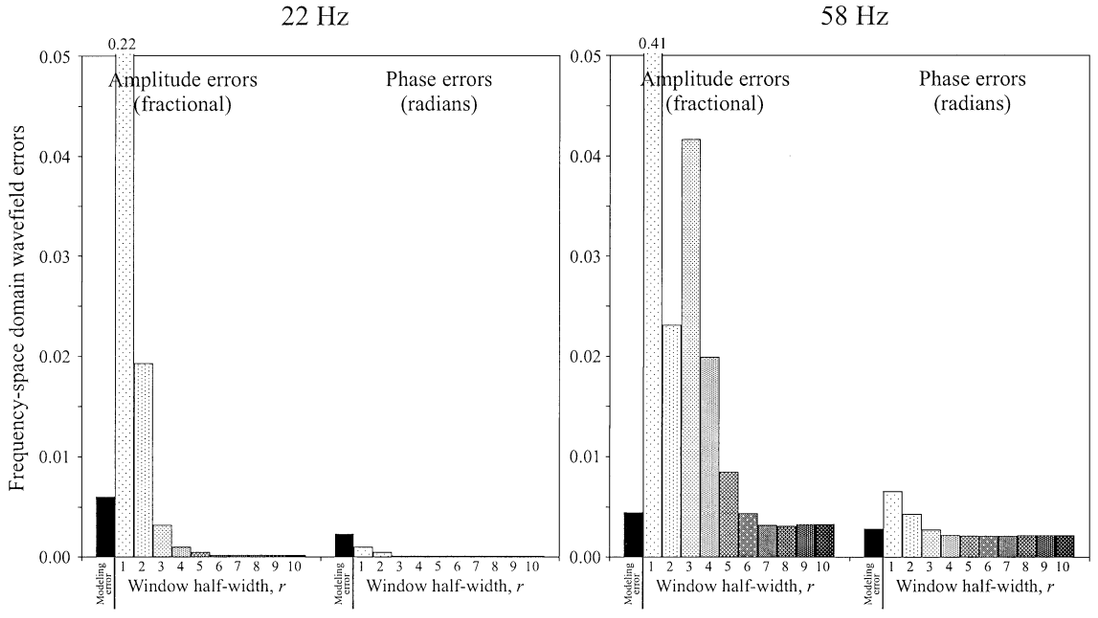

FIG. 7. Amplitude and phase errors 250 m from the source at two different frequencies and for a source and receiver located midway between modeling nodes. The two sets of optimal Kaiser windowing parameters given in Table 1 were used. The modeling errors indicated by the first (black) bars are repeated from Figure 6.

$b = 6.31$, was used except in Figures 8c and 8e, where a source of finite spatial extent (half-width one node spacing) was used. Table 3 lists modeled amplitudes and phases (at 22 Hz) for these different source configurations. These results are given as absolute values rather than as errors, as there is no obvious reference case [in all cases either the source(s) or receivers are located between nodes]. However, from the results presented in Figure 6 we can be confident that the modeling results for Figure 8a are reasonably accurate.

In Figure 8c the contributions at the central node cancel, resulting in two sources two nodes (20 m) apart. Similarly in Figure 8e the node on the free surface cannot contribute to the source function because pressure must be zero there. Hence, in both cases we effectively obtain a source located one node, rather than one-half node, below the free surface. Consequently, both the amplitudes and phases given in Table 3 for Figures 8c and 8e differ significantly from those obtained using any of the other configurations.

For Figure 8d the source terms that would otherwise be above the free surface, and hence outside the model, must be reflected back inside the model with a change of sign. This is equivalent to the change of sign applied to the image source in Figure 8b, the source region of which combines with that of the original source in a manner identical to the way the reflected source terms combine with those located below the free surface. In Figure 9 this procedure is illustrated for a point source located one-half node spacing below a free surface, as in Figure 8d. When modeling in elastic media, the reflected body forces in the vertical component retain their original polarity, while the polarity of the horizontal components are reversed (Cunha, 1993). Although this operation mimics the effect of a mirror-type free surface, its application does not imply that this type of free surface should be used in the finite-difference scheme.

The similarity of the results obtained using Figure 8d to those obtained using either Figure 8a or 8b demonstrates that accurate results can be obtained for a source located arbitrarily close to a free surface. The largest difference between these results is in the amplitudes 50 m below the free surface. This is the result of close proximity of the receiver to the edge of the source region (or vice versa).

CONCLUSIONS

A band-limited delta function can be used to locate both sources and receivers between finite-difference nodes. An appropriate approximation of a band-limited delta function can be obtained by optimal windowing of a sinc function. The shape of a Kaiser window is controlled by only a single parameter, so an optimal band-limited delta function can be rapidly determined via a single parameter search. Moreover, a single windowed sinc function can be used for all internodal source/receiver positions and for all the wavenumbers of interest when using contemporary finite-difference schemes.

The numerical results presented show that, using the method developed, smaller errors are obtained than if sources/receivers are located at the nearest node or are given a finite spatial extent. Errors for the latter are expected to be even

Table 3. Amplitudes and phases of five 22-Hz wavefields, recorded at various distances (in meters) below a free surface. Figure 8 depicts how the source and free surface are represented for the five sets of results given below.

	a		b		c		d		e	
Distance	Amp.	Phase	Amp.	Phase	Amp.	Phase	Amp.	Phase	Amp.	Phase
50	1117.52	2.7627	1117.74	2.7635	1060.49	2.7462	1109.93	2.7603	1052.92	2.7428
100	782.59	−0.1241	781.80	−0.1232	737.77	−0.1320	781.62	−0.1225	737.62	−0.1311
150	635.87	−2.9757	634.50	−2.9743	598.02	−2.9803	633.89	−2.9802	597.50	−2.9864
200	547.84	0.4685	546.39	0.4691	514.69	0.4646	546.51	0.4650	514.78	0.4605
250	486.32	−2.3689	485.86	−2.3710	457.55	−2.3745	489.13	−2.3680	460.62	−2.3714
300	444.95	1.0672	446.41	1.0665	420.42	1.0636	446.96	1.0834	420.90	1.0808

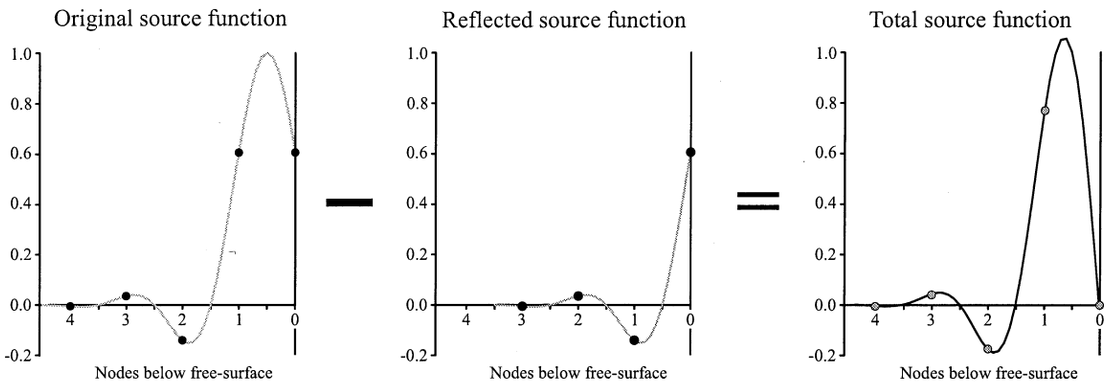

FIG. 9. Illustration of how source terms should be constructed in the vicinity of a free surface. The source terms, as sampled by the modeling grid for a source located one-half node spacing below a free surface, are indicated by circles for a windowed sinc function obtained with $r = 4$ and $b = 6.31$. The source terms that would otherwise be above the free surface are reflected back inside the model and subtracted from the original source terms.

more significant when modeling dipole sources, as required for many types of source in an elastic medium, because a dipole source requires a minimum spatial half-width of two node spacings—twice that of a monopole source (Aboudi, 1971).

Since the model must be homogeneous within each source/receiver region (corresponding with the spatial extent of the windowing function), it is desirable that this distance be as small as possible. Acceptable errors are obtained when source/receiver regions with a half-width as small as four node spacings are used; this half-width may be reduced if the maximum wavenumber of interest is reduced. This is a significant improvement over both the method of Mittet and Arntsen (1999), for which an operator half-width of eight to ten nodes is apparently required, and the initial value method, for which it is usually required that the model be homogeneous for a distance greater than both the length of the finite-difference stencil and that of half a complete wavelet from the edge of the source insertion region.

Sources can be located arbitrarily close to a free-surface boundary in the finite-difference scheme by reflecting back inside the model all the source terms that would otherwise be located above the free surface. This represents a significant improvement over both the initial value method, for which sources must be located sufficiently deep so that no free-surface interaction occurs during the time over which the source is active, and the method of Landrø et al. (1993), for which amplitudes were underestimated when modeling with a free surface.

Although the numerical results presented were obtained by modeling in an acoustic medium, application to elastic media is identical, except that separate source and receiver functions are required for each component of the wavefield. The method developed is attractive because it applies in many general situations, easy to implement, and requires a negligible amount of computation.

ACKNOWLEDGMENTS

Thanks to Gerhard Pratt for his comments, suggestions, and encouragement. This research was supported financially by the Natural Sciences and Engineering Research Council of Canada.

REFERENCES

Aboudi, J., 1971, Numerical simulation of seismic sources: Geophysics, **36**, 810–821.
Alford, R. M., Kelly, K. R., and Boore, D. M., 1974, Accuracy of finite-difference modeling of the acoustic wave equation: Geophysics, **39**, 834–842.
Alterman, Z. S., and Aboudi, J., 1970, Source of finite extent, applied fource and couple in an elastic half-space: Geophys. J. Roy. Astr. Soc., **21**, 47–64.
Alterman, Z., and Karal, F. C., 1968, Propagation of elastic waves in layered media by finite difference methods: Bull. Seis. Soc. Am., **58**, 367–398.
Cole, J. B., 1994, A nearly exact second-order finite-difference time-domain wave propagation algorithm on a coarse grid: Comp. in Phys., **8**, 730–734.
Cunha, C. A., 1993, Elastic modeling in discontinuous media: Geophysics, **58**, 1840–1851.
Dablain, M. A., 1986, The application of high-order differencing to the scalar wave equation: Geophysics, **51**, 54–66.
Holberg, O., 1987, Computational aspects of the choice of operator and sampling interval for numerical differentiation in large-scale simulation of wave phenomena: Geophys. Prosp., **35**, 629–655.
Jo, C.-H., Shin, C., and Suh, J. H., 1996, An optimal 9-point, finite-difference, frequency-space, 2-D scalar wave extrapolator: Geophysics, **61**, 529–537.
Kaiser, J. K., 1974, Nonrecursive digital filter design using the I_0-sinh window function: Int. Symp. on Circuits and Syst., IEEE, Proceeding, 20–23. (Reprinted in Oppenheim, A. V., Ed., 1976, Selected papers in digital signal processing, II: IEEE press, 123–126).
Kurkjian, A. L., Coates, R. T., White, J. E., and Schmidt, H., 1994, Finite-difference and frequency-wavenumber modeling of seismic monopole sources and receivers in fluid-filled boreholes: Geophysics, **59**, 1053–1064.
Landrø, M., Mittet, R., and Sollie, R., 1993, Implementing measured source signatures in a coarse-grid, finite-difference modeling scheme: Geophysics, **58**, 1852–1860.
Mittet, R., and Arntsen, B., 1999, General source and receiver positions in coarse-grid finite-difference schemes: 69th Ann. Internat. Mtg., Soc. Expl. Geophys., Expanded Abstracts, 1855–1858.
Oppenheim, A. V., and Schafer, R. W., 1989, Discrete-time signal processing: Prentice-Hall, Inc.
Pratt, R. G., and Worthington, M. H., 1990, Inverse theory applied to multi-source cross-hole tomography, part I: Acoustic wave-equation method: Geophys. Prosp., **38**, 287–310.
Robertsson, J. O. A., Levander, A., and Holliger, K., 1996, A hybrid wave propagation simulation technique for ocean acoustic problems: J. Geophys. Res., **101**, 11225–11241.
Štekl, I., 1997, Frequency domain seismic forward modelling: A tool for waveform inversion: Ph.D. thesis, University of London.
Štekl, I., and Pratt, R. G., 1998, Accurate viscoelastic modeling by frequency-domain finite differences using rotated operators: Geophysics, **63**, 1779–1794.
Sun, R., and McMechan, G. A., 1987, Line sources for seismic modeling by finite-differences in inhomogeneous media: Geoexploration, **24**, 183–196.

APPENDIX A

COMPARISON WITH THE METHOD OF MITTET AND ARNTSEN (1999)

Mittet and Arntsen (1999) recognized that a discrete band-limited delta function could be used to locate a source between nodes, and they used a least-squares inversion strategy to optimally determine the coefficients of this function. By recognizing that such a function corresponds with a suitably windowed sinc function and that the same Kaiser window can be used for all internodal source locations and for a large range of wavenumbers, I show how Mittet and Arntsen's inversion procedure can be significantly simplified and its robustness increased.

Mittet and Arntsen (1999) proposed inverting for the coefficients d_n, for which $D(k)=1$, $\partial_k D(k)=0$, and $\sum_n d_n = 1$, where $D(k)$ is the complex wavenumber response of d_n. The error function they sought to minimize is

$$\epsilon = \left[\left[\int_{k_{min}}^{k_{max}} \mathrm{d}k|D(k) - 1 + k\partial_k D(k)|^2\right] + \beta\left[\left(\sum_{n=-r}^{r} d_n\right) - 1\right]\right]^2 \qquad \text{(A-1)}$$

[equation (9) in Mittet and Arntsen (1999)]. I suggest that when inverting for an optimal windowing function, only the first condition ($D(k)=1$) need be required. If d_n is based on a symmetrically windowed sinc function, it has a smoothly varying

amplitude response and a near-optimal phase response, regardless of the details of the windowing used. The second condition ($\partial_k D(k) = 0$), which helps guarantee that $D(k)$ is smooth, is therefore no longer required. The third condition ($\sum_n d_n = 1$) was included by Mittet and Arntsen to guarantee a correct amplitude response for the dc component of the source wavelet. This term is redundant because the dc component is included in the first condition when $k = 0$. Furthermore, rather than performing an inversion for all the coefficients of d_n, I only invert for the Kaiser windowing parameter b. The optimum coefficients of d_n can therefore be found very rapidly using a single parameter search.